Point contacts at the CIGS interface - a theoretical outlook

Adrien Bercegol[1],* Binoy Chacko[1],† Reiner Klenk[1], Iver Lauermann[1], Martha Ch. Lux-Steiner[1], and Matthias Liero[2]
[1] *Helmholtz-Zentrum Berlin für Materialien und Energie, Albert Einstein Straße 15, 12489 Berlin, Germany and*
[2] *Weierstraß-Institut für Angewandte Analysis und Stochastik, 10117 Berlin, Germany*

(Dated: April 8, 2016)

For a long time, it has been assumed that recombination in the space-charge region of CIGS is dominant, at least in high efficiency solar cells with low band gap. The recent developments like KF post deposition treatment and point-contact junction may call this into question. In this work a theoretical outlook is made using three-dimensional simulations to investigate the effect of point-contact openings through a passivation layer on CIGS solar cell performance. A large set of solar cells is modeled under different scenarios for the charged defect levels and density, radius of the openings, interface quality and conduction band offset. The positive surface charge created by the passivation layer induces band bending and this influences the contact (CdS) properties, making it beneficial for the open circuit voltage and efficiency, and the effect is even more pronounced when coverage area is more than 95 %, and also makes a positive impact on the device performance, even in the presence of a spike at CIGS/CdS heterojunction.

I. INTRODUCTION

With the advent of post deposition potassium fluoride (KF) treatment in CIGS technology, a new door is opened in the research arena and efficiency catches up to 21.7 % narrowing the gap between the strongest competitor multi-crystalline silicon [1–4]. This finding suggests the role of the interface as a limiting factor for the efficiency and triggered the inevitability of engineering the CIGS/CdS interface for an enhanced device performance, which leads to implement the concept of localized openings through a passivation layer (PL). The idea is inspired by silicon solar technology that already benefited from the micron-sized point contacts to increase its electrical properties [5, 6]. In CIGS, the need of a high-quality interface is particularly important, because of the high density of interface states that can act as the main recombination channel to the device and limit the open-circuit voltage and also the efficiency [7]. By introducing the PL, the area of contact between the CIGS/CdS, is reduced which in turn limits the recombination depending on how effectively the PL passivates the defects.

The concept of passivated emitter and rear cells (PERC) has previously been introduced at the interface at the back contact (CIGS and Mo), witnessing an increase in the efficiency and Voc, but this was limited to ultra-thin films only, as the back contact recombination in standard CIGS (2-3 μm) is negligible due to the gallium grading and photo generation of carriers at the junction is highly probable [8]. The well-established patterning techniques presently used in silicon solar cell for passivation are difficult to employ at the chalcopyrites junction due to the rough surface of the polycrystalline material and because of the shorter diffusion lengths that forces one to make nanometer-scale openings. However, the idea of a point junction was reported by Fu et al. by incorporating ZnS nanodots into In_2S_3 buffer layer, which has been shown to be beneficial for CIGS perfomance [9]. Recently, a novel surface nano patterning technique achieved by self-assembling of alkali condensates make this a method to look for accomplishing PL at CIGS front interface [10].

From these pioneering works, the benign effect of passivation is unequivocal that makes PL a promising way to achieve a high efficiency CIGS solar cell. Even though the point contacts are realized experimentally to some extent, a theoretical investigation is necessary to understand their behaviour and influence on the performance of the device. In this article, different configurations of the point contacts at the CIGS/CdS interface are considered and simulated using two finite-element method (FEM) software tools.

II. MODELS

The FEM software tools employed in this simulation are the two/three-dimensional WIAS-TeSCA [11] and one-dimensional SCAPS [12] that simulate the transport of charge carriers by solving a system of drift diffusion equations. The Shockley-Read-Hall model (SRH) is used to model the recombination through interface and bulk states. Since this study is mainly focused on the influence of the parameters close to the interface, meshing is made considerably denser in this region (about 3.000 points/10.000). The current density versus voltage graphs (J-V) have been realized with a spectrum containing one wavelength of 650 nm and an intensity of 83.1 mW/cm^2. All results are matched with SCAPS

* adrien.bercegol@polytechnique.edu; Also at École polytechnique, Route de Saclay, 91120 Palaiseau, France
† Also at Free University Berlin, D-14195 Germany

if PL is not introduced, omitting in SCAPS as well as in WIAS-TeSCA : reflection loss, ZnO optical loss, and series resistance.

The solar-cell model is a typical CIGSe solar cell to which a 15 nm thick PL is added at the front contact. A 2 μm thick CIGS absorber layer with band gap energy of 1.15 eV, 50 nm CdS buffer layer and a ZnO window layer of 200 nm were implemented. The model parameters for these layers are given in Table 3. The investigated model has three-dimensional cylindrical symmetry with the center of the point contact on the rotation axis. The cell radius, "β", is kept constant, while "α", the contact radius is varied. (see Fig 1)

FIG. 1. Three dimensional sketch of a point-contact CIGS solar cell. α : contact radius, variable, β : cell radius, constant at 500 nm. (a) Three dimensional overview ; (b) Cylindrical cut ; (c) Defect structure at the CIGS front interface

Interfaces studied in this work are modeled by very thin layers containing a high density of defects N_d. These 2 nm thick layers (underlayer/overlayer) are equivalent to the surface recombination model, with surface density N_s yielding : $N_s[cm^{-2}] = 2 * 10^{-7} * N_d[cm^{-3}]$. These equivalent surface densities are given in Table 3. With the introduction of the PL, three interfaces are formed :

- CdS/PL interface, which is assumed to be free of defects
- contact interface (CIGS/CdS) including CIGS overlayer
- passivated interface (CIGS/PL) including CIGS overlayer and ZnS underlayer.

The underlayers/overlayers have a high density of neutral defects N_s^N energetically close to the CIGS mid-gap in common, inducing a high recombination velocity S_{rec}, defined through : $S_{rec} = \sigma * v_{th} * N_s^N$. The defect capture cross section σ =$10^{15} cm^{-2}$ is the same for electrons and for holes.

We considered a wide-band gap semiconductor ZnS as the PL. Different scenarios were simulated at the passivated interface : either donor/acceptor pairs of defects or donor defects only. Defect densities N_s^D (N_s^A) and energetic levels E_d^D (E_d^A) have also been varied following a precise pattern. In contrast to the neutral ones in the CIGSe over layer, these defects can also ionize, creating a positive surface charge across the interface between CIGSe and PL. Fig 1.c shows a zoom on the CIGS front interface, and highlights the position of the defects. The CIGS overlayer corresponds to the red crosses in the diagram, whereas PL underlayer is marked by the white crosses in black background. In summary, our model includes deep charge neutral, recombination inducing defects over the whole area consisting of the PL and contact interfaces. However, only the PL interface can in addition hold an electric charge in specific defects. In addition to the electronic properties of the PL, its geometry was also a parameter considered in this model. The contact area radius, α, was varied from 2 nm to 400 nm, while the distance between the contact radius remains constant, which is valued to be $2\beta = 1\mu m$. Thus the percentage of covered area is given by : $\Pi = 1 - \alpha^2/\beta^2$

In order to see the extent to which the passivation layer can be beneficial to the solar cell, different sets of parameters mentioned above are investigated along with two distinct conduction band offsets at CIGS/CdS interface and two different interface crystalline qualities. By taking all into account, mainly four different types of solar cells have been investigated. As explained in Table I, S_1 (resp. S_2) refers to positive conduction band offset (CBO) (spike at CIGS/CdS) and high (resp. low) recombination velocity S_{rec}, whereas C_1 and C_2 refer to the cell with a cliff at CIGS/CdS, i.e. with negative CBO.

CBO and S_{rec}	$5 * 10^4 cm.s^{-1}$	$2 * 10^5 cm.s^{-1}$
0.1 eV (spike)	S_1	S_2
-0.1 eV (cliff)	C_1	C_2

TABLE I. Matrix showing the four investigated solar cells. CBO refers to conduction band offset at CIGS/CdS. S_{rec} refers to interface recombination velocity

III. RESULTS

The results obtained for the PL featuring the best electronic properties will be presented first, by focusing first on the band diagrams and then on the whole device performance. To which extent other electronic

properties lead to worse results or not, will be explained next.

FIG. 2. Band diagramm for a point-contacted solar cell. Cross-section along the z-axis close to the interface at the contact (blue curve) and on the passivation layer (red curve). $\alpha = 250nm$, and PL includes N_s^D=$2 * 10^{14}/cm^2$ density of donor traps energetically close to the CIGS conduction band. The simulated cell includes a 0.1eV cliff at CIGSe/CdS and $S = S_{max} = 2 * 10^5 cm/s$.

The band diagram close to the interface at z=0, as a function of perpendicular distance to the interface is shown in Fig 2. The plots of the bands are obtained by two vertical cross sections, taken at the contact (blue) and through the PL (red). A big spike at the interface on the conduction band shows the current blocking behavior of the PL. Furthermore, the additional band bending generated at the CIGS/PL interface is clearly visible. The band bending is stronger at the PL than at the contact by more than 0.2 eV. In the vicinity of the PL, the CIGS Fermi-level is closer to the conduction band than at the CIGS/CdS interface.

Fig 3 displays the potential and electron current density direction for α = 50nm, and indicates a potential gradient at the CIGS/CdS interface. To have a better overview of the Fermi-level position at the interface, a horizontal cross section of the valence band is taken across the contact and the PL, and α is varied from 10 nm to 400 nm. This is depicted in Fig 4. The corresponding values of band bending in Table II are obtained by taking the deviation between the valence band energetic level in the bulk ($Ev_{bulk} = -0.19eV$) and just below the interface at the PL (Ev_{PL}) and at the contact (Ev_C). We define then

FIG. 3. Potential (color scale) and electron current (arrows) for α = 50nm. $z = 0\mu m$ corresponds to the CIGS front interface.

FIG. 4. Distance from valence band to Fermi-level 2 nm below the CIGS front interface. $\alpha \in [10, 400]$. PL defect structure, interface recombination velocity and CBO at CIGSe/CdS similar to Fig 2.

$$\phi_{PL} = Ev_{bulk} - Ev_{PL} \text{ and } \phi_C = Ev_{bulk} - Ev_C$$

The transition between ϕ_{PL} and ϕ_C takes place on the contacted area : the PL pins the Fermi level over its full width. Furthermore, an increase in ϕ_C happens when α shrinks and a noticeable change appears when $\Pi > 96\%$.

α (nm)	Π (%)	ϕ_C (eV)	ϕ_{PL} (eV)
10	> 99	0.82	0.85
50	99	0.81	0.85
100	96	0.68	0.85
250	75	0.61	0.85
400	36	0.60	0.85

TABLE II. Band bendings calculated for the simulated cell in Fig 4. Π is the percentage of passivated area, ϕ_C is the band bending at the contact center, ϕ_{PL} at the passivation layer

The open-circuit voltage, being an indicator of recombination, is displayed in Fig 5. A significant reduction of recombination is achieved by the PL. When α is shrinking, Π is growing and V_{oc} is increasing independent of the quality of the solar cell considered at the beginning. It is evident that all $V_{oc}(\alpha)$ curves converges to the same limit for small α. The efficiency also follows the same trend. Fig 6 shows us the limits of efficiency for a point contact junction solar cell, valid for any interface recombination velocity and conduction band offset at CIGSe/CdS. Again, as α gets smaller, the dots representing each investigated device, are getting closer. However, a threshold value appears for the contact radius, from which the efficiency starts to shrink again. As to give a summary of the results featured in Fig 5 & 6, Figure 7 recalls the beneficial effect of the PL featuring the best investigated defect structure, in terms of V_{oc} and efficiency.

After this broad overview of the best cells in the wide range of defect structures investigated in this study, results for all of them are displayed in Fig 8. Five kinds of defect structures have been analyzed, and the results of simulations with PL having same defect structure are aligned, showing that band bending at the passivation layer ϕ_{PL} is independent of S_{rec} and CBO. From Table II, it can be concluded that ϕ_{PL} is also independent of α . To sum up :

$$\frac{\partial \phi_{PL}}{\partial \alpha} = \frac{\partial \phi_{PL}}{\partial CBO} = \frac{\partial \phi_{PL}}{\partial S_{rec}} = 0$$

Hence, it is taken as discriminating factor here. Its influence on the open-circuit voltage and efficiency is significant. Independent of the values of S_{rec} and CBO at CIGSe/CdS, $V_{oc}(\phi_{PL})$ and $\eta(\phi_{PL})$ are increasing functions. However, a PL inducing a weak ϕ_{PL} , corresponding to a weak surface charge leads to a less efficient solar cell. This fact is more pronounced in cells with good quality absorbers, where efficiency drops by 30 %. Also, a certain discrepancy in the results exists around the value of $\phi_{PL} = 0.65eV$. This is due to the parasitic behavior of the traps, which not only bend the bands, but also act as recombination center. In this case, their beneficial effect on the cell performance is mitigated. Still, for $\alpha = 100nm$, $\phi_{PL} \geq 0.85eV$, and for each value of (S_{rec},CBO), the PL significantly enhances the device performance, with at least a 10% increase in efficiency.

FIG. 5. Open circuit voltage for different values of α. High (dotted lines) and low (solid lines) recombination velocity, 0.1eV spike (blue empty shapes) and 0.1 eV cliff (red full shapes) at CIGSe/CdS interface simulation results are being displayed in this figure. The PL includes N_s=$2 * 10^{14}/cm^2$ density of donor traps energetically close to the CIGS conduction band. $\alpha = 500nm$ corresponds to the unpassivated device.

IV. DISCUSSION

The calculations confirm that an additional PL at the top of the absorber has a beneficial effect on the open-circuit voltage and efficiency of the whole device, as long as :

- $\Phi_{PL} > 0.85eV$, i.e. sufficient band bending is generated by the PL
- $\Pi > 95\%$, i.e. more than 95% of the interface is passivated. In our case, this corresponds to $\alpha \leq 50nm$

As already stated in the last section, $\Phi_{PL} > 0.85eV$ only depends on the type of defect structure formed at CIGS/PL. An ideal PL should induce a high density of donor defects or donor/acceptor pairs, energetically located close to the CIGS conduction band [13]. This will generate an electric field at the CIGS/PL interface which drives the electron and repels the holes from the vicinity of the PL, thus mitigating the main recombination channel. Once the new equilibrium is established, the electrons will get to the contacts through diffusion .

In addition to this, a wide range of defect structures were also investigated, resulting in $\phi_{PL} < 0.85eV$, which

FIG. 6. Minimum and maximum efficiency for different values of α. Same set of parameters as in Fig 5

FIG. 7. J-V curves for unpassivated solar cells (dotted lines), and for passivated solar cells (solid lines). $\alpha = 50nm$ and PL includes N_s=$2 * 10^{14}/cm^2$ density of donor trap energetically close to CIGS conduction band.

leads to smaller improvements or even deteriorating the solar cell performance. This emphasizes that main parameter describing the influence of the PL is the band bending it induces. Given that $\Pi > 95\%$, the electric field generated by the PL will also repel the holes from the contact area, as it happens for PERL in ultra-thin films [14]. In fact, we already noticed

FIG. 8. Influence of ϕ_{PL} on V_{oc} and efficiency. $V_{oc,0}$ and η_0 (dotted lines) for unpassivated device performance. High (circles) and low (triangles) recombination velocity, 0.1eV spike (blue empty shapes) and 0.1eV cliff (red full shapes) at CIGSe/CdS interface are displayed. $\alpha = 100nm$, so Π is 96%.

that $\lim_{\alpha \to 0} \phi_C = \phi_{PL}$. Hence, for sufficient small α, not only the CIGS/PL interface but also the CIGS/CdS interface is fully inverted. However, when α gets to the nanometer scale, fill factor loss and series resistance appear, in good correlation with [15]. It is clear from the presented simulations that the fill factor loss occurs because of a drop in the short-circuit current. They also highlight that the threshold value for α is shifted to smaller values when the electronic properties of the PL are optimal. In any case, Π should remain under 99% to avoid fill factor loss. In the simulations presented here, a distance between point contacts that remained in the same order of magnitude as the electron diffusion length was used ($2\beta = 1\mu m$), which is also highly important for the efficiency of a point-contacted structure [14].

The impact of these results extends to most of the CIGS solar cells. Extreme cases were handled for the conduction band offset at CIGSe/CdS and the interface quality, but the results are in all likelihood also true for

intermediate values of these parameters. Varying the CBO between CIGS and CdS has a drastic influence on the initial solar cell performance. Without any passivation layer, avoiding a barrier reduction at the interface between CIGS and CdS maximizes the effective band gap seen by the numerous interface recombination sites [16]. As described by dotted lines in Figure 7, a cliff induces an even more direct dependence between defect density and open-circuit voltage losses, which is also assessed by [17]. Still, intrinsic donor traps located at the interface could correct this negative effect [18]. In our study, these traps don't come from the intrinsic interface between CIGS or CdS, but directly from the interface between CIGSe and PL. They generate the full type inversion already described before, completely annihilating the negative influence of a cliff at the interface between CIGS and CdS. With this knowledge, the need for a buffer layer, the main feature of which is to align the band between CIGS and window layer [19], could be called into question. However, the modeling of surface recombination through a thin layer with high N_d could be the reason for these results, which doesn't take into account tunneling recombinations between charge carriers coming from different layers [11].

Concerning the interface recombination velocity, which was varied from a rather low value to a fairly high value, the PL can mitigate its influence, though not in the same extent as the CBO. Even for an ideal PL, V_{oc} and η don't catch up to the same values. This can be explained by the fact that no perfect passivation of the defects is assumed here, unlike Reinhard et al. [10], who modeled the interface between PL and CIGSe without any defects. It is very noteworthy that a significant improvement also occurs for a device having initially a very small interface recombination rate, the efficiency of which should theoretically be limited by recombination in the quasi-neutral region [7, 20].

The strong band bending in the absorber towards the interface (and the resulting type inversion) is the most important parameter mitigating the influence of interface recombination. It can happen due to the diffusion of the atomic elements into the Cu vacancies in the CIGS absorbers, like the Zn diffusion from the ZnS passivation layer [21] or the removal of Cu from the interface and occupation of potassium in the KF treatment [10]. An appropriate etching completely removes the surface oxides before the chemical bath deposition of the buffer layer. [22] Hence the Na segregation on top of the CIGS layer, that also leads to interface passivation, has not been considered.

The results give a frame for experimental implementation of the PL. It highlights the fact that the most efficient passivation layer works through field-induced passivation. Instead of looking at the defect density or the defect energetic level, the surface charge density at CIGS/PL should be investigated for any efficiency improvement. Therefore, thickness of the PL plays no influence, and this is confirmed with simulation results (not shown here) done by varying the PL thickness.The PL is more beneficial to a bad quality absorber (cliff at CIGS/CdS), and their use would make the development easier of efficient PL.
An optimum buffer layer, in addition to appropriate band line-up, should also generate shallow defects at the interface carrying the required positive charge. The standard CdS buffer layer might do so via ionized Cd within the Cu-free surface reconstruction of CIGS [23]. As our model includes charged defects only at the PL but not at the contact interface, it may be argued that the benefit of the PL layer is exaggerated. However, additional calculations (not shown here) suggest that a cell with full area contact even with charged defects will still be worse than the point contact cell, in particular with the cliff-type band alignment. If nothing else, using two different materials (contact, PL) to fulfill one requirement (band line-up, positive charge) each should provide more flexibility in designing the best possible interface.

V. CONCLUSION

From a large spectrum of solar cells considered in the simulation, nano-contacts through a passivation layer at CIGS front interface has shown a benign effect on the performance of the device, independent of the quality of the interface. With the introduction of the PL, appearance of the positive charge bends the band at the CIGS/PL interface leading to an n-type inversion in this region, significantly influences the contact area properties when the coverage area of PL is greater than 95%. The positive impact of PL also extends to cells having a favorable conduction band offset at CIGS/CdS interface. These findings call into question the role of buffer layer and allow a greater flexibility for trying out different buffer layers. The numerical simulation also underline the promising feature of point contacts structures in CIGS technology, and yields vital information for understanding and designing an efficient passivation layer.

VI. ACKNOWLEDGEMENTS

Binoy Chacko would like to thank the Erasmus Mundus scholarship programme for supporting his study at the Freie Universität Berlin and Helmholtz-Zentrum Berlin.

[1] Chirila A., Reinhard P., Pianezzi F., Bloesch P., Uhl A.R., Fella C., Kranz L., Keller D., Gretener C., Hagendorfer H., Jaeger D., Erni R., Nishiwaki S., Buecheler S., Tiwari A.N. Potassium-induced surface modification of Cu(In,Ga)Se2 thin films for high-efficiency solar cells, *Nature Mater.*, vol. 12, 1107-1111 (2013)

[2] Green M. A., Emery K., Hishikawa Y., Warta W., Dunlop E. D. Solar cell efficency tables(version 45). *Progress in Photovoltaics: Res. Appl.*, Vol 23, 1, 19 (2015)

[3] Jackson P., Hariskos D., Lotter E., Paetel S., Wuerz R., Menner R., Wischmann W., Powalla M. New world record efficiency for Cu(In,Ga)Se2 thin-film solar cells beyond 20. 8%. *Progress in Photovoltaics: Res. Appl.* 2011; 19: 894897.

[4] Jackson P., Hariskos D., Wuerz R., Kiowski O., Bauer A., Friedlmeier T. M. and Powalla M. , Properties of Cu(In,Ga)Se2 solar cells with new record efficiencies up to 21.7%. *Phys. Status Solidi RRL*, 9: 2831 (2015)

[5] Zhao J., Wang A., Green M.A., 24% Efficient PERL structure silicon solar cells, *Proceedings of the 21st IEEE PVSC*, 1990, pp. 333335

[6] Giesecke J.A., Kasemann M., Warta W. Determination of local minority carrier diffusion lengths in crystalline silicon from luminescence images. *Journal of Applied Physics*, 106 (2009), pp. 014907014907-8

[7] Scheer R., Schock H.-W. Chalcogenide Photovoltaic : Physics, Technologies, and Thin Film Devices. *Wiley* (2011)

[8] Vermang B., Wätjen J. T., Fjällström V., Rostvall F., Edoff M., Kotipalli R., Henry F., Flandre D. Employing Si solar cell technology to increase efficiency of ultra-thin Cu(In,Ga)Se2 solar cells, *Prog. Photovolt: Res. Appl.*, 22, 10231029 (2014)

[9] Fu Y., Allsop N., Gledhill S.E., Köhler T., Krüger M., Saez-Araoz R., Blöck U., Lux-Steiner M.Ch., Fischer Ch-H. ZnS Nanodot film as Defect passivation layer for CIGS thin-film solar cells deposited by Spray-ILGAR. *Advanced Energy Materials* 561-564 (2011)

[10] Reinhard P., Bissig B., Pianezzi F., Hagendorfer H., Sozzi G., Menozzi R., Gretener C., Nishiwaki S., Buecheler S., Tiwari A. N. Alkali-Templated Surface Nanopatterning of Chalcogenide Thin films : A novel approach towards solar cells with enhanced efficiency. *Nano-Letters*, 15 pp 33343340, (2015)

[11] WIAS-TeSCA. Modeling and simulation of Semiconductor Devices. http://www.wias-berlin.de/software/tesca

[12] Burgelman M., Nollet P. Degrave S. Modelling polycrystalline semiconductor solar cells. *Thin Solid Films*, 361-362, 527-532 (2000)

[13] N.Allsop M., Nürnberg R., Lux-Steiner M. Ch., Schedel-Niedrig Th. Three-Dimensionnal simulations of a thin film heterojunction solar cell with a point contact/defect passivation structure at the heterointerface. *Applied Physics Letters*, 122108, (2009)

[14] Nerat M. CIGS solar cells with localized back contacts for achieving high performance. *Solar Energy Materials* 104 (2012)

[15] Fu Y. Spray-ILGAR deposition of controllable ZnS nanodots and application as passivation/point contact at junction $In_2S_3/Cu(In,Ga)(S,Se)_2$ in thin film solar cells. *Doctoral Thesis*, HZB (2012)

[16] Klenk R. Characterisation and modelling of chalcopyrite solar cells. *Thin Solid Films* 387 (2001)

[17] Minemoto T., Matsui T., Takakura H., Hamakawa Y., Negami T., Hashimoto Y., Uenoyama T., Kitagawa. M. Theoretical analysis of the effect of conduction band offset of window/CIS layers on performance of CIS solar cells using device simulation. *Solar Energy Materials*, 67 pp. 83-88, (2001)

[18] Gloeckler M., Sites J. R. Efficiency limitations for wide-band-gap chalcopyrite solar cells. *Thin Solid Films* 480-481:241-245 (2005)

[19] Platzer-Björkman Ch. Band Alignment Between ZnO-Based and Cu(In,Ga)Se2 Thin Films for High Efficiency Solar Cells. *Doctoral Thesis*, Uppsala University (2006)

[20] Scheer R. Towards an electronic model for $CuIn_{1-x}Ga_xSe_2$ solar cells. *Thin Solid Films* 519, 7472-7475 (2011)

[21] Cojocaru-Miredin O., Fu Y., Kostka A., Saez-Araoz R., Beyer A., Knaub N., Fischer Ch-H., Raabe D. Interface engineering and characterization at the atomic-scale of pure and mixed ion layer gas reaction buffer layers in chalcopyrite thin film solar cells. *Progress in Photovoltaics, Res. Appl.* 23, 705-716 (2015)

[22] R. Hunger, T. Schulmeyer, M. Lebedev, A. Klein, W. Jaegermann, R. hied, M. Powalla, K. Sakurai and S. Niki. Removal of the surface inversion of CIS absorbers by NH3 etching, 3^{rd} *world conference on energy conversion* May 2003, Osaka, Japon

[23] Kiss J., Gruhn T., Roma G., Felser C. Theoretical study on diffusion mechanism of Cd in the Cu-poor phase of CuInSe2 Solar Cell Material. *J. Phys. Chem.* 117, 25933-25938 (2013)

Layer properties	CIGSe	CdS	PL	i-ZnO	ZnO
$thickness$	2	0.05	0.015	0.05	0.2
$N_{D/A}$ cm^{-3}	$N_A : 10^{16}$	$N_D : 4 * 10^{15}$	$N_D : 10^{15}$	$N_D : 10^{18}$	$N_D : 10^{18}$
ϵ/ϵ_0	13.6	13.6	8.3	9	9
E_g eV	1.15	2.4	3.6	3.3	3.4
χ eV	4.5	4.4/4.6 ⋆	3.9	4.4	4.4
N_c cm^{-3}	$7 * 10^{17}$	$4 * 10^{18}$	$6 * 10^{18}$	$4 * 10^{18}$	$4 * 10^{18}$
N_v cm^{-3}	$1.5 * 10^{19}$	$9 * 10^{18}$	$6 * 10^{19}$	$9 * 10^{18}$	$9 * 10^{18}$
μ_n $cm^2V^{-1}s^{-1}$	100	100	100	100	100
μ_p $cm^2V^{-1}s^{-1}$	25	25	25	25	25
τ_n ns	50	33	∞	10	10
τ_p ns	50	0.033	∞	0.01	0.01
v_{th} $cm.s^{-1}$	10^7	10^7	10^7	10^7	10^7
Interface properties	CIGSe/CdS	CIGSe/PL Donor		CIGSE/PL Donor/Acceptor	
N_s^N cm^{-2}	$5 * 10^{12}/2 * 10^{13}$ †	$5 * 10^{12}/2 * 10^{13}$ †		$5 * 10^{12}/2 * 10^{13}$ †	CIGS ⋄
E_d^N eV	0.55	0.55		0.55	overlayer
N_s^D cm^{-2}	0	$2 * 10^{10}/2 * 10^{12}/2 * 10^{14}$ ‡		$2 * 10^{13}$	ZnS ⋄
E_d^D eV	0	0.08		0.13/0.33 ‡	underlayer
N_s^A cm^{-2}	0	0		$2 * 10^{13}$	ZnS ⋄
E_d^A eV	0	0		0.08/0.28 ‡	underlayer

TABLE III. Simulation input parameters. d : thickness, $N_{D/A}$: Doping, E_g : band gap, χ : electron affinity, N_c/N_v : density of states, μ : mobility, τ : bulk lifetime, N_s^N / E_d^N : Neutral defect density and energetic level below CIGSe conduction band, N_s^D / E_d^D / N_s^A / E_d^A : same for donor and acceptor traps. ⋆ CBO variation ; † S variation ; ‡ Defect structure variation ; ⋄ Defect position, see Fig 1.c

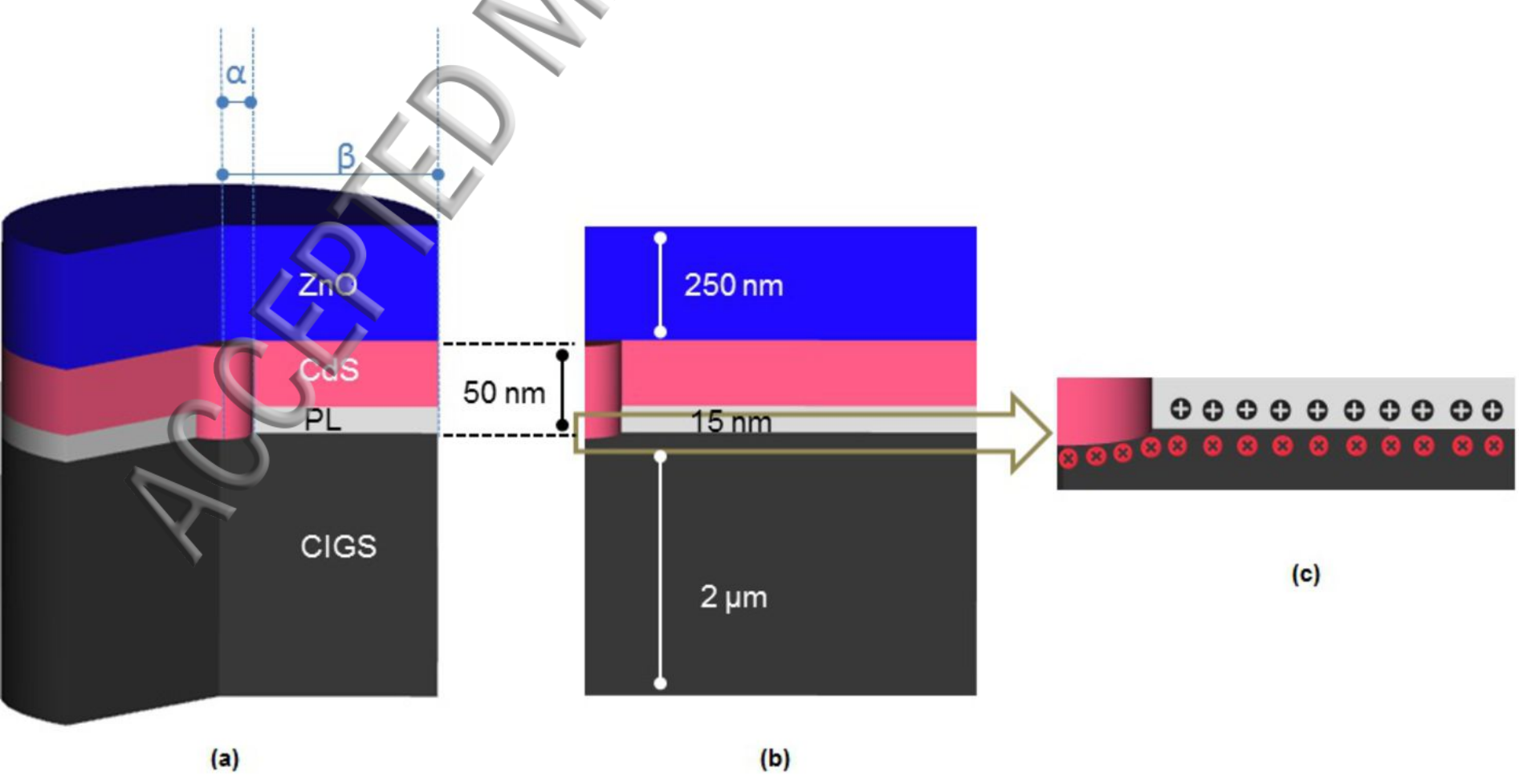

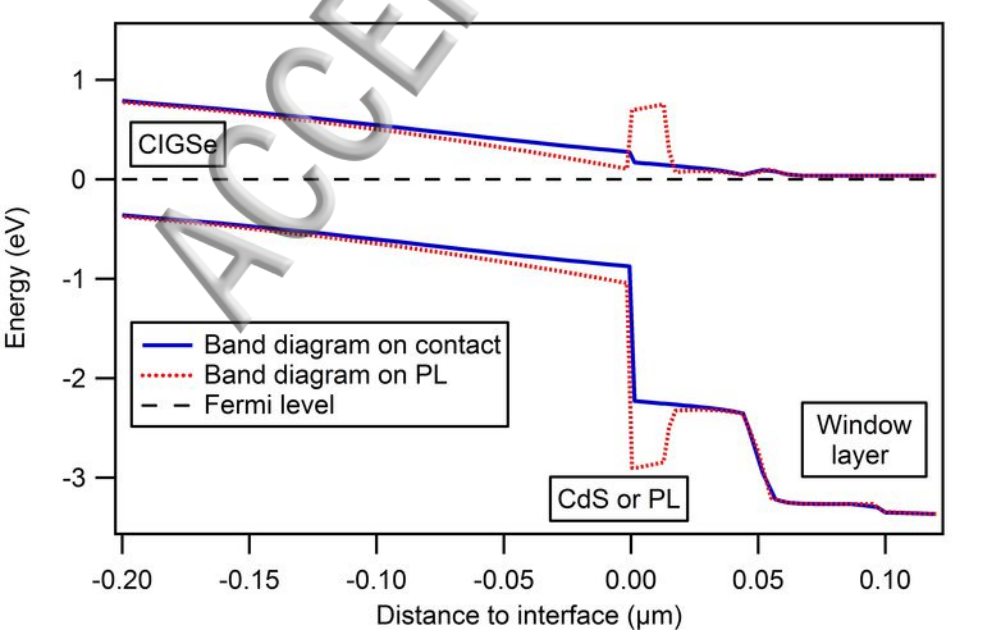
CIGSe
Band diagram on contact
Band diagram on PL
Fermi level
CdS or PL
Window layer
Energy (eV)
1
0
-1
-2
-3
-0.20
-0.15
-0.10
-0.05
0.00
0.05
0.10
Distance to interface (μm)

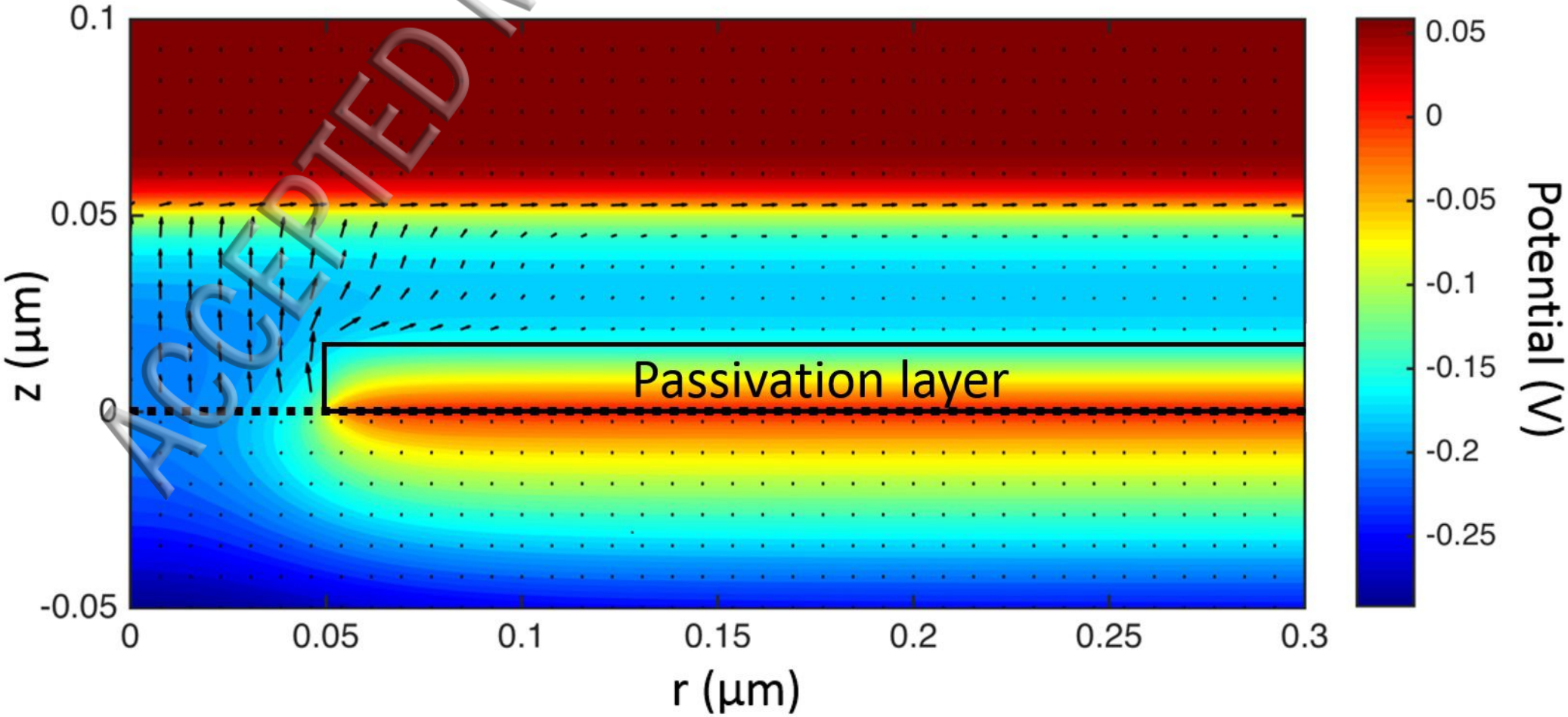
0.1
0.05
0
-0.05
z (μm)
0
0.05
0.1
0.15
0.2
0.25
0.3
r (μm)
Passivation layer
0.05
0
-0.05
-0.1
-0.15
-0.2
-0.25
Potential (V)

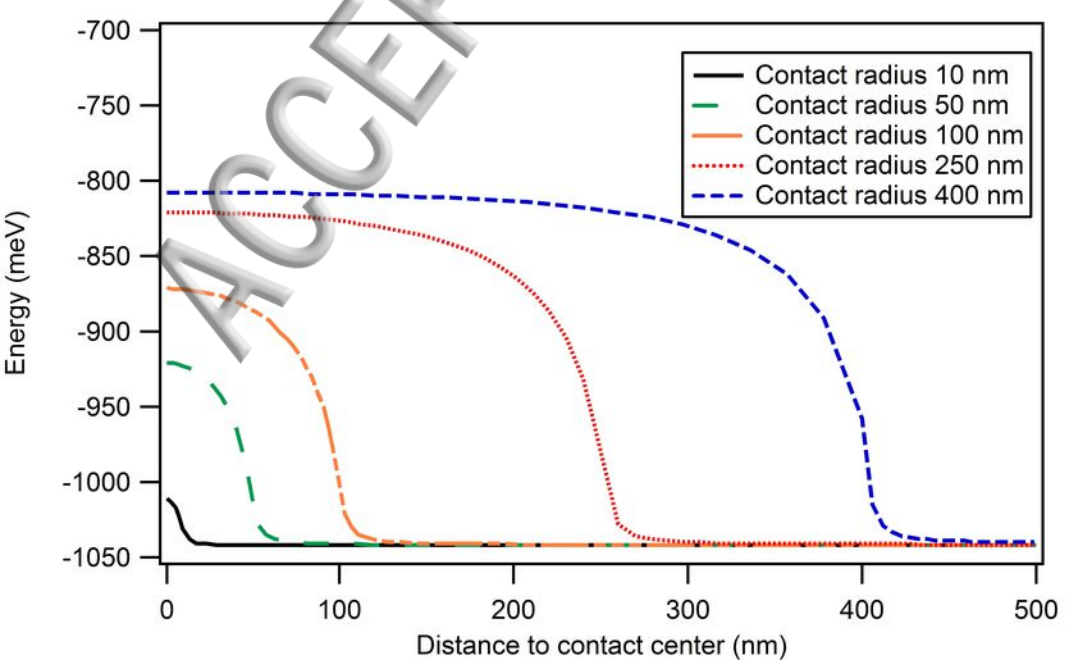
Contact radius 10 nm
Contact radius 50 nm
Contact radius 100 nm
Contact radius 250 nm
Contact radius 400 nm
Energy (meV)
-700
-750
-800
-850
-900
-950
-1000
-1050
0
100
200
300
400
500
Distance to contact center (nm)

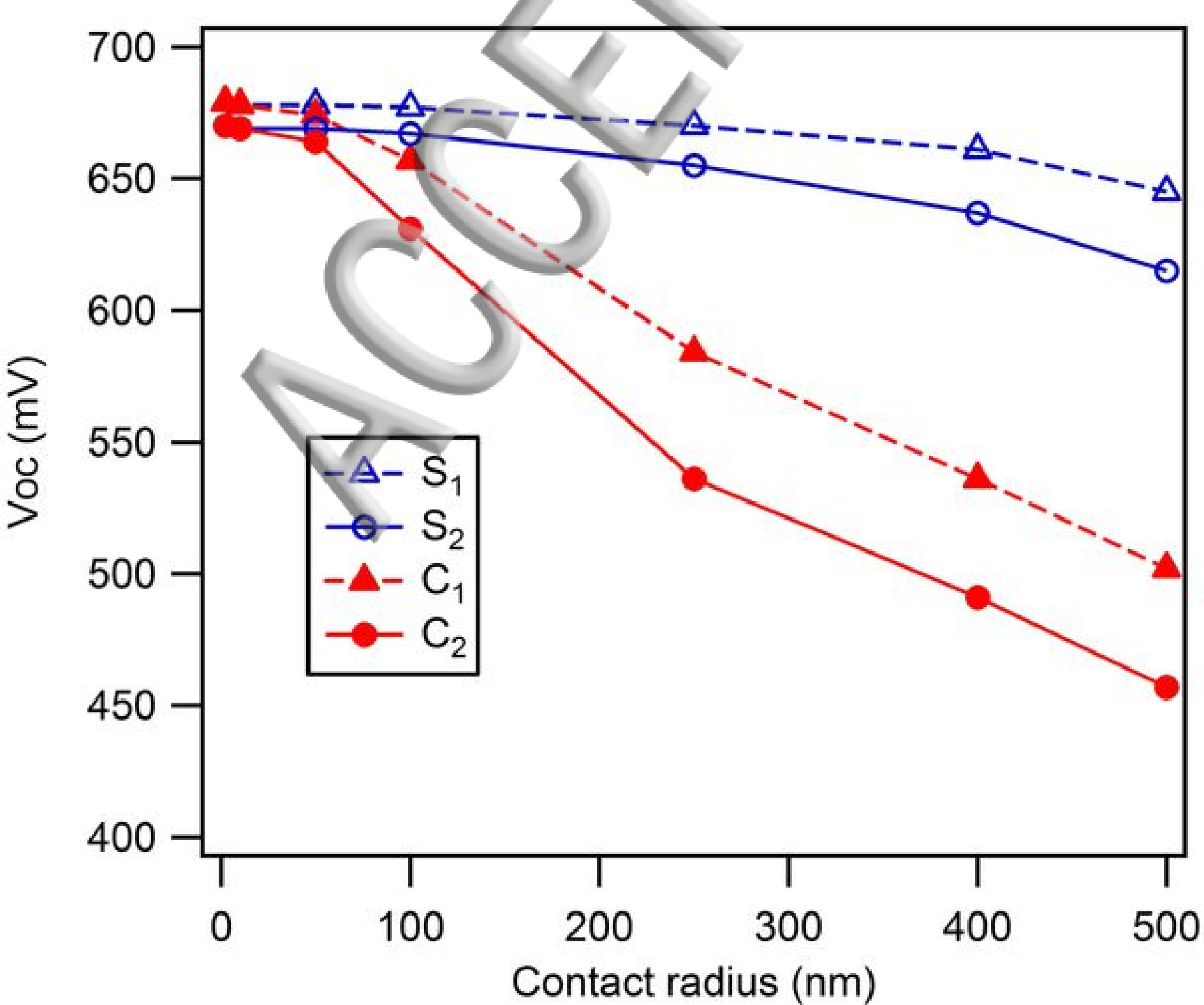
700
650
600
550
500
450
400
Voc (mV)
0
100
200
300
400
500
Contact radius (nm)
S1
S2
C1
C2

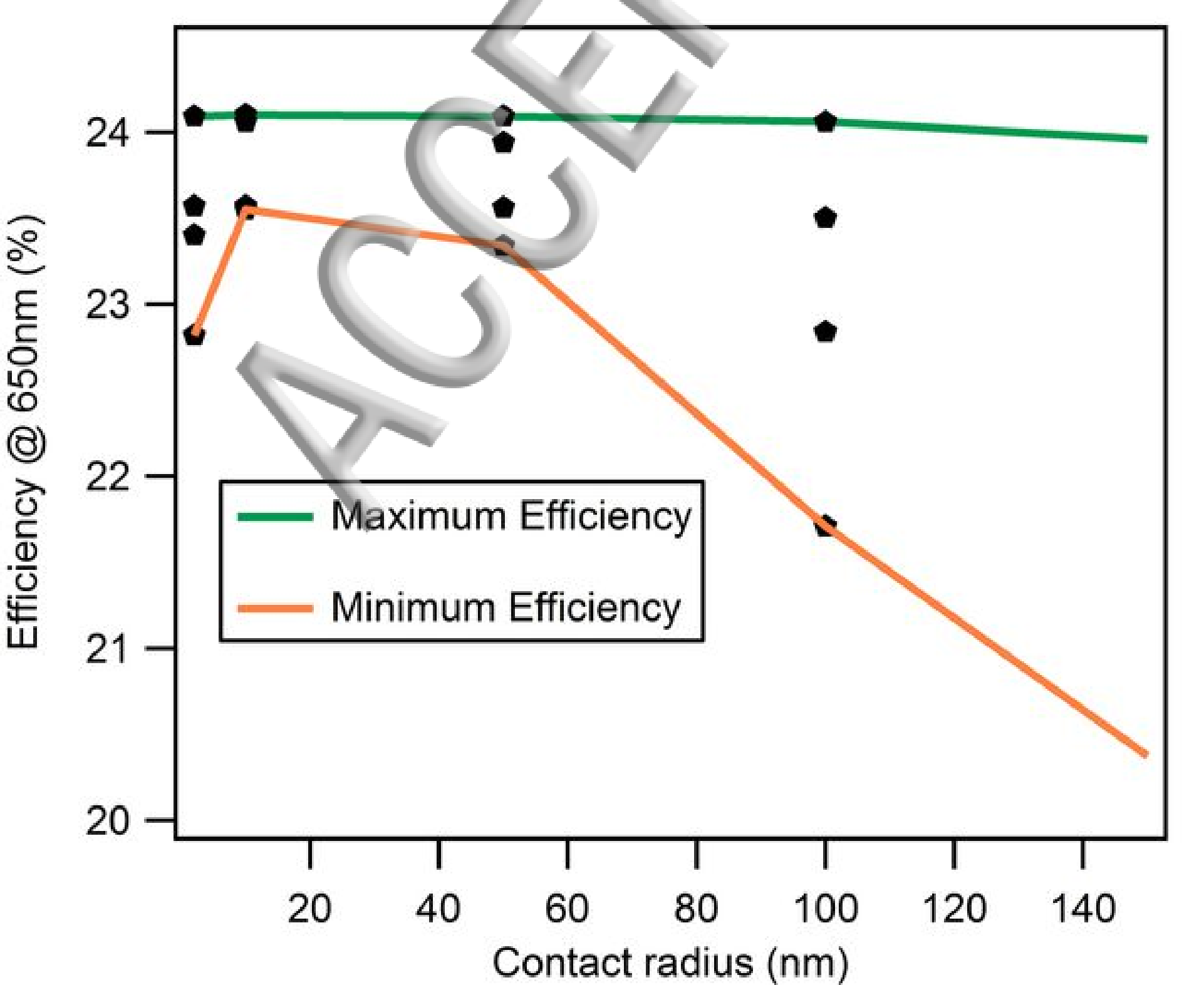
Efficiency @ 650nm (%)
24
23
22
21
20
20
40
60
80
100
120
140
Contact radius (nm)
Maximum Efficiency
Minimum Efficiency

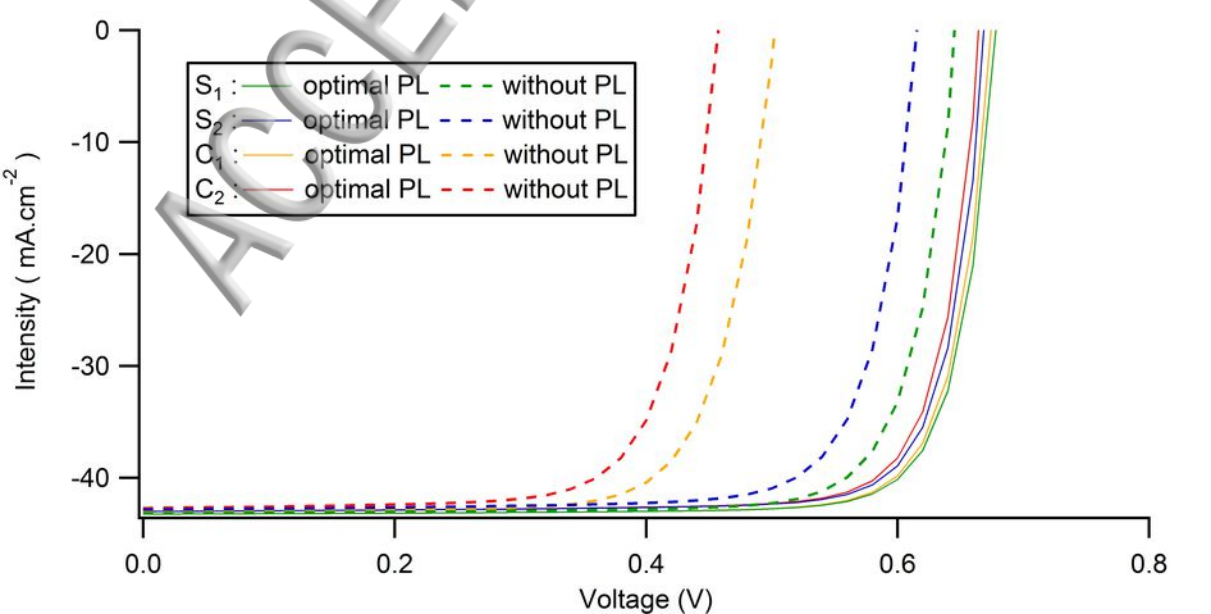
S1 : optimal PL without PL
S2 : optimal PL without PL
C1 : optimal PL without PL
C2 : optimal PL without PL
Intensity (mA.cm-2)
0
-10
-20
-30
-40
0.0
0.2
0.4
0.6
0.8
Voltage (V)

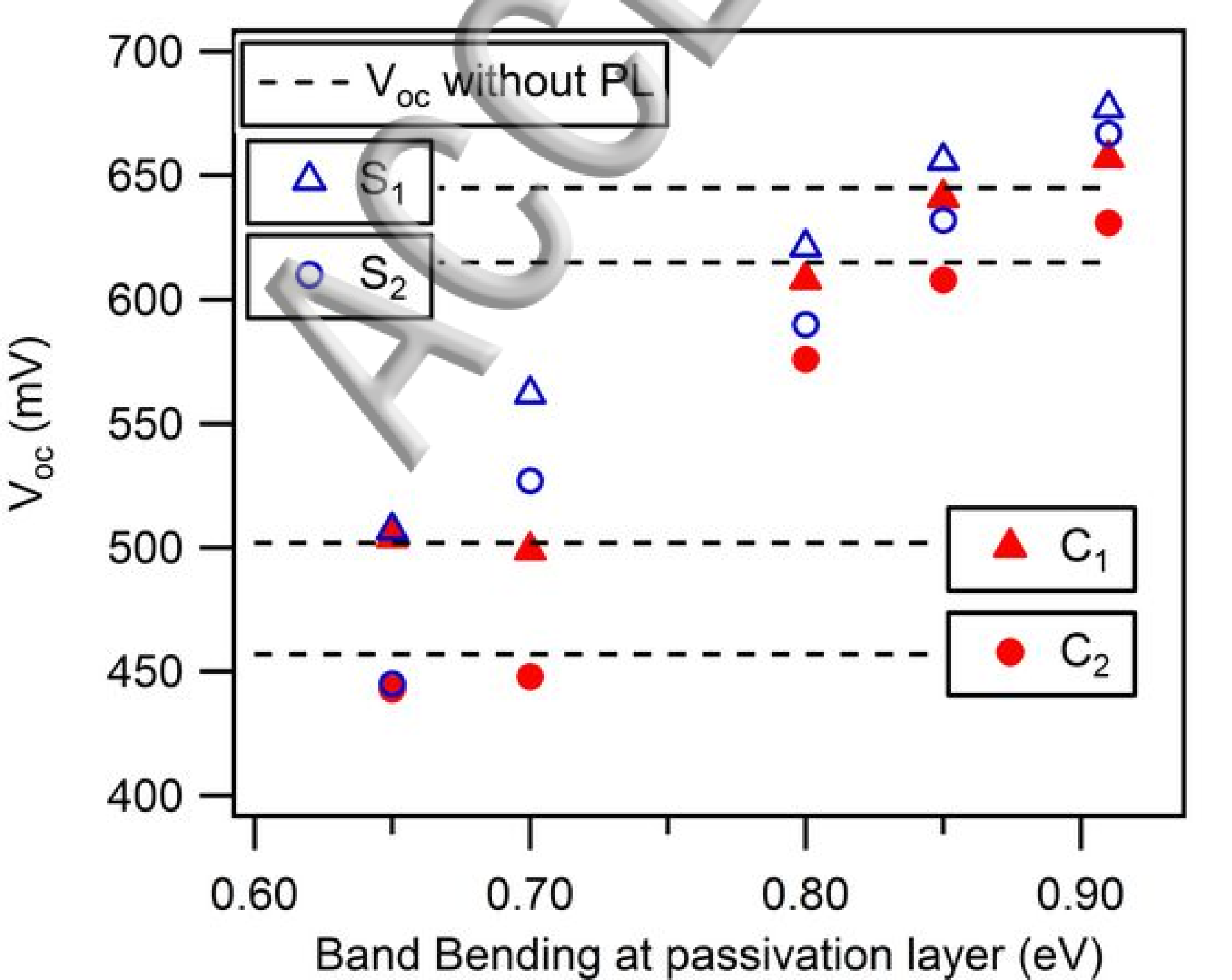
700
650
600
550
500
450
400
V_{oc} (mV)
V_{oc} without PL
S_1
S_2
C_1
C_2
0.60
0.70
0.80
0.90
Band Bending at passivation layer (eV)

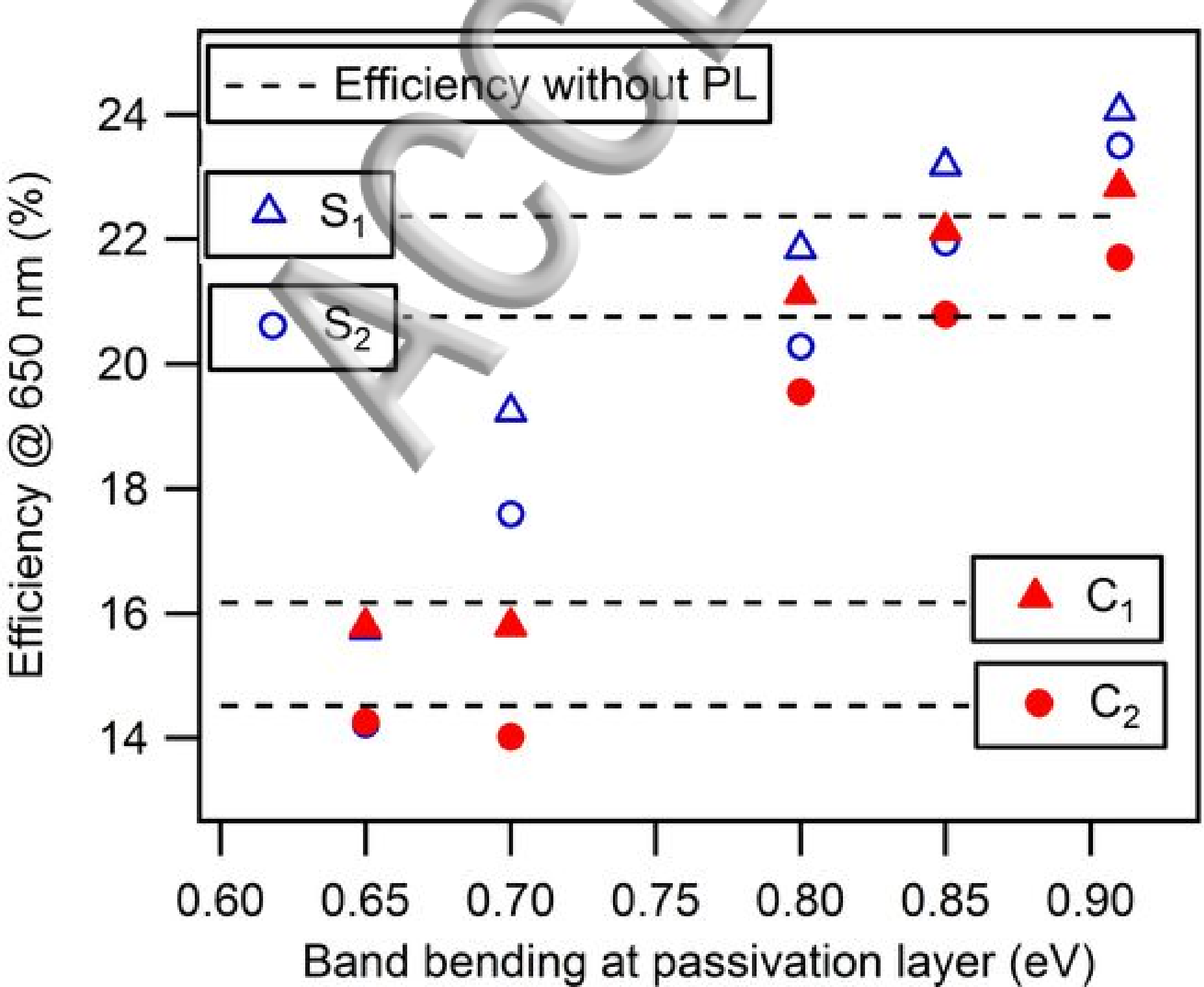
Efficiency without PL
S1
S2
C1
C2
Efficiency @ 650 nm (%)
24
22
20
18
16
14
0.60
0.65
0.70
0.75
0.80
0.85
0.90
Band bending at passivation layer (eV)